
Scalable Hybrid HMM with Gaussian Process Emission for Sequential Time-series Data Clustering

Yohan Jung
KAIST

Jinkyoo Park
KAIST

Abstract

Hidden Markov Model (HMM) combined with Gaussian Process (GP) emission can be effectively used to estimate the hidden state with a sequence of complex input-output relational observations. Especially when the spectral mixture (SM) kernel is used for GP emission, we call this model as a hybrid HMM-GPSM. This model can effectively model the sequence of time-series data. However, because of a large number of parameters for the SM kernel, this model can not effectively be trained with a large volume of data having (1) long sequence for state transition and 2) a large number of time-series dataset in each sequence. This paper proposes a scalable learning method for HMM-GPSM. To effectively train the model with a long sequence, the proposed method employs a Stochastic Variational Inference (SVI) approach. Also, to effectively process a large number of data point each time-series data, we approximate the SM kernel using Reparametrized Random Fourier Feature (RRFF). The combination of these two techniques significantly reduces the training time. We validate the proposed learning method in terms of its hidden-state estimation accuracy and computation time using large-scale synthetic and real data sets with missing values.

1 Introduction

A sequence of time-series data is ubiquitous. Such a sequence of time-series data can often describe the evolution of the hidden state of a target system. For example, a sequence of blood pressure or heartbeat time-series can represent the health condition of a patient. Therefore, infer-

ring the hidden state of a target system using a sequence of time-series has long been an important research topic in engineering and science.

HMM is a model designed to specify the varying hidden states for sequential data. HMM has been mainly applied to classifying human action, speech, and DNA sequence [1, 2, 3, 4, 5], which are all related to understanding the evolution of target system characteristics over time. In general, HMM consists of two-part; The transition model considers Markov's dynamic of discrete hidden state, and the emission model considers the likelihood of the observed data in a given hidden state. Since the emission model of vanilla HMM has a limitation in expressing complex observations because of its simple assumption, Hybrid HMM whose emission considers a nonlinear function such as neural net (NN), has been devised [6, 7, 8, 9, 10]. However, even though Hybrid HMM shows better performance with improved modeling power, it still has limitations in applying to incomplete data with missing values [11].

To address this problem, HMM using GP as the emission has been considered because GP has excellent expressive power as well as a nonparametric characteristic of GP enables the combined model applicable to the data containing missing values. As examples of these attempts, Nakamura uses Semi-HMM with GP emission to classify dynamic motion [12]. Zitao also conducts a study that leads to improved clinical time-series data prediction by combining GP with the emission of the Kalman filter, a continuous hidden state version of HMM [13]. Regarding time-series data, Hensman proposes a hierarchical model that combines the Dirichlet process with a GP mixture model, which clustered gene expression time-series data with missing values [14]. However, these studies consider the commonly used RBF kernel, the Periodic kernel, and the combination of them. Since choosing a kernel is what determines the covariance structure of the GP that describes the data, choosing the kernel should be considered more carefully.

One way to solve the mentioned issue is to employ a Spectral Mixture (SM) kernel that can approximate any stationary kernel [15]. It has also shown excellent performance when modeling time series data sets. Ulrich et al. [16, 17] propose an Infinite HMM whose emission consists of the

Mixture of Experts model using Multi-output GP with each output being modeled by a spectral mixture kernel. Then, the proposed model is used to analyze human brain signals that change over time. Their approach classifies human brain signals over time into distinct hidden states, which could be described by different covariances characterized in the spectral domain. However, this model can not be scalably trained with large scale time-series dataset because many parameters of SM kernel tend to require extensive training time and induce over-fitting.

In this paper, we first introduce the hybrid HMM with GP Emission using spectral mixture kernel, which is a simplified version of Ulrich’s model for sequential single output time-series data. Then, we propose a scalable learning method of the introduced model for large sequential time series data. Specifically, we employ Stochastic Variational Inference (SVI) based on [18, 19, 20] to efficiently process the long sequence of state-transition if long sequence dataset is given. Also, we develop Spectral Kernel Approximation by Reparameterized Random Fourier Feature (R-RFF) to efficiently process a large number of observations (≥ 1000) observed at each state. This approximation can reduce computational cost to optimize kernel hyperparameters for GP emission. As a result, the combination of these two methods enables our introduced model to train a large volume of the dataset.

Also, we validate the classification performance of the model trained by our proposed method on large-scale data containing missing values.

2 Background

We first discuss the model structures for HMM and GP. In addition, we discuss the background on the SM kernel and Random Fourier Feature (RFF) technique for approximating the SM kernel.

2.1 Hidden Markov Model (HMM)

HMM is a probabilistic model to depict the sequential observations obtained under the varying hidden state of a target system. HMM consists of a transition model describing the transition of the hidden state over time and an emission model depicting the probability distribution of the observations given the hidden state. For the transition of the hidden state, the Markov assumption is used.

Let $Y = \{y_t\}_{t=1}^T$ be observations measured at each t time and $Z = \{z_t\}_{t=0}^T$ be the corresponding the discrete hidden states where $z_t \in \{1, \dots, K\}$. Then, the joint distribution of hidden state and observation of HMM is expressed as :

$$p(Z, Y) = \pi_0(z_0) \prod_{t=1}^T p(z_t | z_{t-1}, A) p(y_t | z_t) \quad (1)$$

where A is the transition matrix of hidden states that $A_{i,j}$ represents the probability of the transition from $z_{t-1} = i$ to $z_t = j$, i.e. $Pr(z_t = j | z_{t-1} = i) = A_{i,j}$. The θ denotes the parameter of emission. The initial parameter π_0 plays role in setting where the hidden state occurs at the first time. For the emission $p(y_t | z_t)$, Gaussian or Mixture of Gaussian distribution is usually used in case of continuous observations. To relax the over-fitting problem in training HMM, Bayesian HMM considers the parameters $\{\pi, A, \theta\}$ as random variable and aims to infer these variables using observations. Typically, Dirichlet distribution (Dir) and Normal-inverse-Wishart distribution (NIW) are assumed as the prior distribution for the parameters π, A and θ , respectively.

To train HMM, the Expectation Maximization (EM) is applied, which alternatively optimizes the parameters of distributions for the hidden state and the emission model. This alternation respectively corresponds to updating local variables and global variables. For the Bayesian HMM, Variational Bayes EM (VBEM) and Markov Chain Monte Carlo (MCMC) are used for training [21, 22].

2.2 Gaussian Process (GP)

GP is a stochastic process which assumes that any finite random variables of the stochastic process follow Gaussian distribution. GP can be used as a prior for a function that explains the relation between input and output [23]. Let x and y be the pair of inputs and outputs and let f be target function with GP prior assumption to consider the relation between x and y .

$$y = f(x) + \epsilon, \quad \epsilon \sim N(0, \sigma_\epsilon^2) \quad (2)$$

$$f(x) \sim GP(m(x), k(x, x'; \theta)) \quad (3)$$

where $m(x)$ denotes the mean function of f . The kernel function $k(x, x'; \theta)$ defines $\text{cov}(f(x), f(x'))$ by the inputs x, x' and the hyperparameter θ .

The kernel hyperparameter θ is trained by maximizing the log marginal likelihood $\log p(Y|X)$ for the given inputs $X = \{x_n\}_{n=1}^N$ and outputs $Y = \{y_n\}_{n=1}^N$ with the number of dataset N .

$$\begin{aligned} \log p(Y|X) = & -\frac{1}{2} Y^T (K_{X,X} + \sigma_\epsilon^2 I)^{-1} Y \\ & - \frac{1}{2} \log |K_{X,X} + \sigma_\epsilon^2 I| - \frac{n}{2} \log 2\pi \end{aligned} \quad (4)$$

where $K_{X,X}$ is the evaluation of kernel function over X , i.e. $[K_{X,X}]_{ij} = k(x_i, x_j)$.

2.3 Spectral Mixture Kernel (SM)

For the stationary kernel which assumes that covariance between $f(x_1)$ and $f(x_2)$ for any inputs $x_1, x_2 \in \mathbb{R}^P$ is invariant to translation of the inputs, i.e. $\text{cov}(f(x_1), f(x_2)) = k(|x_1 - x_2|, 0)$ [24].

By Bochner's theorem, stationary kernel $k(\tau)$ can be obtained by taking the Fourier transform to spectral density of $S(s)$ for target function f where $\tau = |x_1 - x_2|$ between two inputs x_1 and x_2 .

$$k(\tau) = \int e^{-2\pi i s^T \tau} S(s) ds \quad (5)$$

This theorem implies that if $S(s)$ approximates well the empirical spectral density of observations $\{y_t\}_{t=1}^T$ of f , the corresponding kernel of target function f can be obtained by applying Fourier transform to the $S(s)$. Wilson [15] implements this idea to generate a new kernel known as the spectral mixture kernel (SM kernel).

This approach first represents the spectral density $S(s) = \frac{1}{2}(\psi(s) + \psi(-s))$ using the weighted sum of Gaussian distribution $\psi(s)$ to define the induced $k(\tau)$ on a real domain.

$$\psi(s) = \sum_{q=1}^Q w_q N(s|\mu_q, \Sigma_q) \quad (6)$$

where $\mu_q = (\mu_q^{(1)}, \dots, \mu_q^{(P)})$ and $\Sigma_q = \text{diag}(\nu_q^{(1)}, \dots, \nu_q^{(P)})$. Putting $S(s)$ into the equation (5) leads the SM kernel defined as

$$k_{SM}(\tau) = \sum_{q=1}^Q w_q \cos(2\pi \tau^T \mu_q) \prod_{p=1}^P \exp(-2\pi^2 \tau_p^2 \nu_q^{(p)}) \quad (7)$$

where τ_p is the p th components in the $\tau \in \mathbb{R}^P$.

2.4 Sparse Spectrum GP Approximation by Random Fourier Feature (RFF)

2.4.1 Random Fourier Feature (RFF)

Random Fourier Features method has been proposed to reduce the computation cost in the kernel learning domain [25]. This method approximates the kernel function $k(x - y)$ by applying the Monte Carlo integration [26] to the Bochner's theorem (5).

Let $S = \{s_i\}_{i=1}^M$ be the sampled M spectral points from the spectral density $S(s)$. Then, the approximated kernel $\hat{k}(x - y)$ is obtained by the equation :

$$\begin{aligned} k(x - y) &= \mathbb{E}_{s \sim S(s)} [e^{2\pi i s^T (x - y)}] \\ &\approx \frac{1}{M} \sum_{i=1}^M \cos(2\pi s_i^T x) \cos(2\pi s_i^T y) \\ &\quad + \sin(2\pi s_i^T x) \sin(2\pi s_i^T y) \quad (8) \end{aligned}$$

This can also be defined by the inner product of feature map. Let $x_S = [2\pi x^T s_1, \dots, 2\pi x^T s_M]$ be the feature inputs and $\phi_S(x) = \frac{1}{\sqrt{M}}[\cos(x_S), \sin(x_S)] \in \mathbb{R}^{2M}$ be the

feature map. Then the approximated kernel $\hat{k}(x - y)$ can also expressed as $\phi_S(x)\phi_S(y)^T$ based on (8). Then, the corresponding Gram matrix $K_{X,X}$ can be computed as $\Phi_S(X)\Phi_S(X)^T$ where $\Phi_S(X) = [\phi_S(x_1); \dots; \phi_S(x_n)] \in \mathbb{R}^{n \times 2M}$.

2.4.2 Sparse Spectrum Approximation in Gaussian Process

Approximated kernel by RFF can reduce the training and inference time compared with original GP [27].

When the approximate kernel by (8) replace $K_{X,X}$, then the log marginal likelihood (4) is differently computed with the sampled spectral points $S = \{s_i\}_{i=1}^M$.

$$\begin{aligned} \log p(Y|X, S) &= -\frac{1}{2} Y^T (\Phi_S(X)\Phi_S(X)^T + \sigma_\epsilon^2 I)^{-1} Y \\ &\quad - \frac{1}{2} \log |\Phi_S(X)\Phi_S(X)^T + \sigma_\epsilon^2 I| - \frac{n}{2} \log 2\pi \quad (9) \end{aligned}$$

Since the computation of $(\Phi_S(X)\Phi_S(X)^T + \sigma_\epsilon^2 I)^{-1}$ takes $O(nM^2)$ instead of $O(n^3)$ by matrix inversion lemma [28]. We can reduce the computation time when $M \ll n$.

3 Methodology

3.1 Hybrid HMM with GP Emission

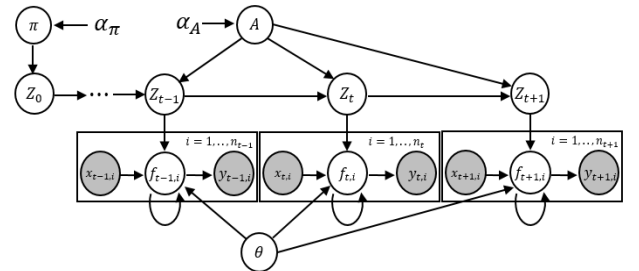


Figure 2: Hybrid HMM with GP Emission

We introduce a hybrid HMM with GP emission using SM kernel designed to classify the hidden state for a sequence of single-output time-series data.

We assume that the output time-series data $\{y_{t,j}\}_{j=1}^{n_t}$ corresponding to time-series inputs $\{x_{t,j}\}_{j=1}^{n_t}$ are obtained every time step t . Here, $x_{t,j}$ and $y_{t,j}$ are the j th input and output given at time t , respectively. $\{y_{t,:}, x_{t,:}\}$ denote the full observations at time t . z_t denotes the corresponding discrete hidden state over $\{y_{t,:}, x_{t,:}\}$ where $z_t \in \{1, \dots, K\}$.

Hybrid HMM with GP emission follows the same structure of vanilla HMM with equation (1) except the emission function. The emission of this model introduces the GP prior on the $f_{t,:}$ to explain the relation between $y_{t,:}$ and $x_{t,:}$.

under the hidden state z_t and SM kernel k_{z_t} as

$$f_{t,:}|x_{t,:}, z_t \sim GP(m_{z_t}(x_{t,:}), k_{z_t}(x_{t,:}, x_{t,:}; \theta_{z_t})) \quad (10)$$

where θ_{z_t} denotes the hyperparameters of the SM kernel k_{z_t} having Q_{z_t} mixture components. In addition, each point in time series is measured with independent and identically distributed (i.i.d.) Gaussian noise as

$$y_{t,i} = f_{t,i}(x_{t,i}) + \epsilon, \quad \epsilon \sim N(0, \sigma_\epsilon^2) \quad (11)$$

Then, the log likelihood of the observation $p(y_{t,:}|x_{t,:}, z_t)$ is computed as the marginalization over the prior $f_{t,:}$: given k_{z_t} as:

$$p(y_{t,:}|x_{t,:}, z_t) = \int p(y_{t,:}|f_{t,:}, x_{t,:}, z_t)p(f_{t,:}|x_{t,:}, z_t)df_{t,:} \quad (12)$$

Additionally, we assume the prior distribution for transition matrix A and initial distribution π where the Dirichlet distribution is assigned to each row of A and π .

$$p(\pi) = \text{Dir}(\pi|\alpha^\pi) \quad (13)$$

$$p(A) = \prod_{i=1}^K \text{Dir}(A_{i,:}|\alpha_i^A) \quad (14)$$

3.2 Variational Bayes Expected Maximisation (VBEM)

HMM with GP emission can be trained by Variational Bayes Expected Maximisation (VBEM). Given the model assumptions for HMM with GP, the log joint likelihood of Z, Y given X is expressed as

$$\begin{aligned} \log p(Z, Y|X) &= \log \pi_0(z_0) + \sum_{t=1}^T \log p(z_t|z_{t-1}, A) \\ &+ \sum_{t=1}^T \log p(y_{t,:}|z_t, x_{t,:}) \end{aligned} \quad (15)$$

In VBEM approach, variational distribution $q(\pi, A, Z)$ are introduced to approximate the posterior $p(\pi, A, Z|Y, X)$. Mean field assumption for $q(\pi, A, Z)$ leads to independent relation for each variable, i.e $q(\pi, A, Z) = q(\pi)q(A)q(Z)$. After we apply the Jensen's inequality to the log marginal likelihood $\int \log p(Z, Y|X)p(\pi)p(A)d\pi dA dZ$, we get the following Evidence Lower Bound \mathcal{L} (ELBO) :

$$\begin{aligned} \mathcal{L}(q(\pi), q(A), q(Z)) &= \mathbb{E}_q[\log p(Z, Y|\pi, A) - \log q(Z)] \\ &+ \mathbb{E}_q[\log p(\pi) - \log q(\pi)] + \mathbb{E}_q[\log p(A) - \log q(A)] \end{aligned} \quad (16)$$

Maximizing the \mathcal{L} is equivalent to minimize the KL divergence between $q(\pi, A, Z)$ and $p(\pi, A, Z|Y, X)$, which results in updating the variational parameters $\{w_\pi, w_A\}$ of global variable $\{\pi, A\}$ and local variable Z alternatively.

The update of local variable $q(Z)$ is induced as follows:

$$\begin{aligned} q^*(Z) &\propto \exp\left(\sum_{t=1}^T \log p(y_{t,:}|z_t, x_{t,:})\right) \\ &+ \mathbb{E}_{q(\pi)}[\log p(z_0)] + \sum_{t=1}^T \mathbb{E}_{q(A)}[\log p(A_{z_{t-1}, z_t})] \end{aligned} \quad (17)$$

To evaluate the updated local variable $q^*(Z)$, the following auxiliary variables $\tilde{\pi}, \tilde{A}_{j,i}$ should be computed.

$$\tilde{\pi} = \exp(\mathbb{E}_{q(\pi)}[\log \pi_j]), \quad \tilde{A}_{j,i} = \exp(\mathbb{E}_{q(A)}[\log A_{j,i}]) \quad (18)$$

Then, forward-backward algorithm using $p(y_{t,:}|z_t, x_{t,:})$, $\tilde{\pi}$ and \tilde{A} generates $q^*(z_i), q^*(z_{i-1}, z_i)$ to be used for the update of global variable parameters.

Updating the global variable parameters is conducted as follows:

$$w_{\pi_j} = \alpha_j^\pi + \mathbb{E}_{q(Z)}[1_{z_0=j}] \quad (19)$$

$$w_{A_{j,i}} = \alpha_{j,i}^A + \sum_{t=1}^T \mathbb{E}_{q(Z)}[1_{z_{t-1}=j, z_t=i}] \quad (20)$$

where w_{π_j} and $w_{A_{j,i}}$ denote variational parameter for j -th element of π and (j, i) element of A . The α_j^π and $\alpha_{j,i}^A$ denote Dirichlet prior for π_j and Dirichlet prior for $A_{j,i}$. The $1_{z_0=j}, 1_{z_{t-1}=j, z_t=i}$ denote the sufficient statistic for $q(\pi)$ and $q(A)$, respectively.

The hyperparameters of SM kernel $\theta = \{\theta_1, \dots, \theta_K\}$ are trained by maximizing the following objective :

$$\begin{aligned} &\sum_{t=1}^T \mathbb{E}_{q(Z)}[\log p(y_{t,:}|z_t, x_{t,:})] \\ &= \sum_{t=1}^T \sum_{j=1}^K \log p(y_{t,:}|z_t = j, x_{t,:})q(z_t = j) \end{aligned} \quad (21)$$

This optimization applies the gradient method such as non-linear conjugate gradients and L-BFGS.

3.3 Scalable Learning

The VBEM method is difficult to employ for training HMM-GP with the SM kernel using the data having 1) long sequence of state transition (T is large), 2) a large number of observations in each time-series (n_t is large), mainly due to a large number of the SM kernel parameters.

To tackle the mentioned issue, we apply Stochastic Variational Inference (SVI) for 1) based on [19, 20], which intend to approximate the ELBO for long sequence data by linear approximation through the sampled short sequence data. For 2), we develop Spectral Kernel Approximation

by Reparameterized Random Fourier Feature (R-RFF) that optimizes SM kernel hyperparameters in a stochastic manner.

3.3.1 SVI Approach

In the SVI approach, we approximate the log likelihood of the total T sequence of time-series data as the log likelihood of uniformly sampled short L sequence of time-series data called by batch data with the single batch sampling.

Given the T sequence of time series observations, we randomly sample L time series observations $Y_L^s = \{y_{i,:}, \dots, y_{i+L-1,:}\}$ corresponding the inputs X_L^s and the hidden states Z_L^s , where the index i is sampled uniformly from $i \in \{1, \dots, T - L + 1\}$.

Since the ELBO for sampled $\{X_L^s, Y_L^s\}$ needs to calibrate in order to replace the ELBO for $\{X, Y\}$, we take linear approximation of ELBO of $\{X, Y\}$ by considering expected log joint likelihood of $\{Z_L^s, Y_L^s\}$ given X_L^s .

$$\begin{aligned} & \mathbb{E}_s \left[\mathbb{E}_q [\log p(Y_L^s, Z_L^s | X_L^s)] \right] \\ & \approx \frac{1}{T - L + 1} \mathbb{E}_q \left[\sum_{t=1}^{T-L+1} \log p(z_{t-1}) + \right. \\ & \left. L \sum_{t=1}^T \log p(A_{z_{t-1}, z_t}) + L \sum_{t=1}^T \log p(y_{t,:} | z_t, x_{t,:}) \right] \quad (22) \end{aligned}$$

By the equation (22), the batch factor c_s^A, c_s^θ to coordinate ELBO of $\{X_L^s, Y_L^s\}$ with full ELBO of $\{X, Y\}$ is obtained as follows:

$$c_s^A = \frac{T - L + 1}{L}, \quad c_s^\theta = \frac{T - L + 1}{L} \quad (23)$$

Applying stochastic natural gradient descent to the natural parameter of variational distribution $q(A), q(\pi)$ iteratively leads to the update rule for the global variable as follows :

$$w_{\pi_j}^{n+1} = (1 - p_n) w_{\pi_j}^n + p_n \left(\alpha_j^\pi + \mathbb{E}_{q(Z^s)} [1_{z_i=j}^s] \right) \quad (24)$$

$$\psi^s = c_s^A \mathbb{E}_{q(Z^s)} \left[\sum_{t=1}^L 1_{z_{i+t-1}^s=j, z_{i+t}^s=k} \right]$$

$$w_{A_{j,k}}^{n+1} = (1 - p_n) w_{A_{j,k}}^n + p_n (\alpha_{j,k}^A + \psi^s) \quad (25)$$

where w_π, w_A are the natural parameter of Dirichlet distribution and p_n is n -th learning rate of stochastic optimization. SM kernel hyperparameters θ are trained by maximizing expected log marginal likelihood λ^s with the batch factor c_s^θ .

$$\lambda_i^s = c_s^\theta \mathbb{E}_{q(Z_L^s)} \left[\sum_{t=0}^{L-1} \log p(y_{i+t,:} | z_{i+t}, x_{i+t,:}) \right] \quad (26)$$

For multiple M batch data $\{Y_L^{s_m}, X_L^{s_m}, Z_L^{s_m}\}_{m=1}^M$, varia-

tional parameters are similarly updated as follows:

$$\tau_j^{s_m} = \mathbb{E}_{q(Z^{s_m})} [1_{z_{m_i}=j}^{s_m}]$$

$$w_{\pi_j}^{n+1} = (1 - p_n) w_{\pi_j}^n + p_n \left(\alpha_j^\pi + \frac{1}{M} \sum_{m=1}^M \tau_j^{s_m} \right) \quad (27)$$

$$w_{A_{j,k}}^{n+1} = (1 - p_n) w_{A_{j,k}}^n + p_n \left(\alpha_{j,k}^A + \frac{1}{M} \sum_{m=1}^M \psi^{s_m} \right) \quad (28)$$

SM kernel hyperparameters are updated by maximizing the following objective:

$$\frac{1}{M} \sum_{m=1}^M \lambda_{m_i}^{s_m} \quad (29)$$

where m_i is first sampled index of m batch data.

Updating the parameters of the local variable is similarly updated as VBEM except that full dataset $\{Y, X\}$ are replaced with sampled $\{Y_L^s, X_L^s\}$.

3.3.2 SM Kernel Approximation for GP Emission

To scale up the GP emission, we approximate the SM kernel by Reparameterized Random Fourier Feature (R-RFF). Then, the approximated SM kernel is employed to regularized sparse spectrum GP approximation for the reduction of computation cost.

Given the parameters of SM kernel $\{w_q, \mu_q, \sigma_q\}_{q=1}^Q$, we sample spectral points from Gaussian distribution $N(S; \mu_q, \sigma_q)$ by reparametrization trick.

$$s_{q,i} = \mu_q + \sigma_q \circ \epsilon_i \quad (30)$$

where $\epsilon_i \sim N(\epsilon; 0, I)$ for $i = 1, \dots, m_q$. The sampled spectral points $\mathbf{s} = \cup_{q=1}^Q \{s_{q,i}\}_{i=1}^{m_q}$ induces the feature map $\phi_{SM}(x)$, which can approximate $k_{SM}(x - y)$.

$$\begin{aligned} \phi_{SM}(x) &= [\sqrt{w_1} \phi_1(x), \dots, \sqrt{w_Q} \phi_Q(x)] \\ k_{SM}(x - y) &\approx \phi_{SM}(x) \phi_{SM}(y)^T \quad (31) \end{aligned}$$

where $\phi_q(x)$ is the feature map defined by the sampled spectral points $\{s_{q,i}\}_{i=1}^{m_q}$ from $N(S; \mu_q, \sigma_q^2)$ by (8).

Based on Stochastic Gradient Variational Bayes (SGVB) [29], we derive the regularized lower bound of log marginal likelihood with Reparametrized kernel approximation (31).

$$\begin{aligned} & \log p(y_{t,:} | z_t, x_{t,:}) \\ & \geq \int \log p(y_{t,:} | z_t, x_{t,:}, S) q(S) dS - KL(q(S) || p(S)) \\ & \approx \frac{1}{K} \sum_{k=1}^K \log p(y_{t,:} | z_t, x_{t,:}, \mathbf{s}^{(k)}) - KL(q(S) || p(S)) \quad (32) \end{aligned}$$

where $\mathbf{s}^{(k)}$ is repetitive k -th sampled spectral points from $q(S) = \prod_{q=1}^Q N(S; \mu_q, \sigma_q)$ for robust lower bound approximation. $p(S)$ is the prior distribution of spectral density, whose parameter can be tuned by using empirical spectral density. The second term $-KL(q(S)||p(S))$ of this lower bound (32) acts as a regularizer to prevent the spectral density distribution from collapsing in training.

The obtained (32) can be employed as the alternative to $\log p(y_{t,:}|z_t, x_{t,:})$ with less computation.

3.4 Computation Complexity

To analyze the computation complexity of our learning algorithm, we split the algorithm mainly into three parts; computation of log marginal likelihood for observations by GP emission, local update, and global update. We proceed with the analysis of our computation under a single batch assumption because the repetitive sampling for robust SVI and lower bound of log marginal likelihood (32) increases the total computation linearly.

For computing the log marginal likelihood of $T \times n$ observations with K hidden state, the conventional VBEM approach costs $\mathcal{O}(KTn^3)$. Our approach costs $\mathcal{O}(KLnm^2)$, where the length of the sampled sequence is L sequence, and the total m sampled spectral points are used for SM kernel approximation. This is because SVI approach reduces to $\mathcal{O}(L)$ from $\mathcal{O}(T)$ and SM kernel approximation reduces to $\mathcal{O}(nm^2)$ from $\mathcal{O}(n^3)$. For the update of local variables, VBEM and SVI take $\mathcal{O}(K^2T)$ and $\mathcal{O}(K^2L)$ for the forward-backward algorithm, respectively. Updating the global variable is dominated by updating kernel hyperparameters. Computing the derivative of log marginal likelihood for each parameter costs $\mathcal{O}(n^3)$ [23]. Thus, in the case of spectral mixture kernel, VBEM costs $\mathcal{O}((3Q+1)n^3KT)$ where All spectral mixture kernels take Q Gaussian mixture components. However, our scalable approach takes $\mathcal{O}((3Q+1)nm^2KL)$.

In summary, our scalable learning method scalably trains the large dataset when we control m and L such that $nm^2 \ll n^3$ and $L \ll T$.

4 Experiments

We conduct two experiments for validation. In the experiments, the following performance metrics are used to evaluate the performance of the trained models.

- Accuracy : how correct the estimated hidden states match to the true label after reordering the estimated clusters by Munkres algorithm [30]
- Time : training time (seconds) for given dataset
- #Cluster : the number of the estimated hidden states

4.1 Scalable Learning (Q1)

We conduct the first experiment to validate how the proposed learning strategies (SVI and R-RFF) expedite the training of HMM-GPSM with a large volume of data, i.e., 1) long sequence (T is large) and 2) a large number of observations in each time-series (n_t is large).

We use the synthetic sinusoidal dataset for the first experiment. We consider 8 states whose state transition follows a Markov assumption. Specifically, there are two groups of states whose state dynamics are different: (1 \rightarrow 2 \rightarrow 3 \rightarrow 4) and (5 \rightarrow 6 \rightarrow 7 \rightarrow 8). Each state except state 4 in the first group follows the stay probability 0.7 and the move probability 0.3. Similarly, each state except state 8 in the second group has stay probability 0.3 and the move probability 0.7. The special states {4, 8} connect the two group with probability 1, i.e., (4 \rightarrow 5) and (8 \rightarrow 1).

Given a hidden state $s \in \{1, \dots, 8\}$, we assume that the distinct sinusoidal $f_Q^s(t)$ is observed.

$$f_Q^s(t) = \sum_{q=1}^Q \tilde{\alpha}_{s,q} \sin(\omega_{s,q} \pi t) + \epsilon \quad (33)$$

where Q is the number of spectral components for sinusoidal. The frequency components $\omega_{s,q}$ is uniformly sampled from the interval $[0, 20]$. The weight factors $\{\tilde{\alpha}_{s,1}, \dots, \tilde{\alpha}_{s,Q}\}$ are normalized version of $\{\alpha_{s,1}, \dots, \alpha_{s,Q}\}$ where $\alpha_{s,q}$ is uniformly sampled from the $[0, 1]$. This normalization intends to make sure that the statistics such as the mean and standard deviation of each time-series observations are not be a determinant factor to classify the sinusoidal generated in different state.

To investigate the complexity of the spectral pattern, we consider $Q = 3, 6$. In addition, to investigate the impact of the number of time-series measurements, we consider two sampling frequency 200Hz and 1000Hz. For every combination of Q and sampling frequency Hz, we generate a time-series for $2T$ seconds using (33), i.e, $2T \times 200(\text{Hz})$ and $2T \times 1000(\text{Hz})$. Then, we use the first half of them for training ($T \times \text{Hz}$) and the left half of them for test ($T \times \text{Hz}$).

For the comparison of the proposed training methods, we take HMM-GPSM introduced in Figure 2 as the modeling baseline. Then, we compare mainly the following three learning strategies:

- GPSM-VBEM : Bayesian HMM with GP emission model combined with SM kernel trained by VBEM
- GPSM-SVI : Bayesian HMM with GP emission model combined with SM kernel trained by SVI
- GPSM(RSS)-SVI : Bayesian HMM with GP emission model combined with approximated SM kernel trained by SVI

To provide the information of how difficult the distinct sinusoidal data is classified, we also takes following benchmarks models based on HMM:

Methods (#T, #L, #B-K, #SPPt, #SPPt-K)	Accuracy(Q=3)		#Cluster(Q=3)		Accuracy(Q=6)		#Cluster(Q=6)	
	200Hz	1000Hz	200Hz	1000Hz	200Hz	1000Hz	200Hz	1000Hz
KNNDTW	.83	.92	8	8	.62	.69	8	8
HMM-T	.39(.04)	.34(.02)	8	8	.30(.02)	.27(.03)	7.8(.4)	7.8(.4)
HMM-S	.86	.77	8	8	.62(.04)	.42(.09)	8	8
BHMM-T	.48	.46	8	8	.40	.46	8	8
BHMM-S	.89	1.00	8	8	.74	.78	8	7
GPSM-VBEM (100,—,—,—,—)	.82(.06)	—	6.2(.60)	—	.87 (.03)	—	5.6(.40)	—
GPSM-SVI (100,10,1,—,—)	.80(.06)	.82(.06)	6.3(1.0)	5.0(.47)	.84(.06)	.67(.06)	5.4(1.3)	4.0
GPSM-SVI (100,10,3,—,—)	.80(.06)	.82(.10)	6.1(1.0)	5.2(1.0)	.81(.06)	—	5.4(.92)	—
GPSM(RSS)-SVI (100,10,1,5,2)	.86(.04)	.90(.07)	6.3(1.0)	6.7(1.0)	.78(.07)	.77(.05)	5.0(.77)	5.3(.64)
GPSM(RSS)-SVI (100,10,3,5,2)	.86(.08)	.92(.07)	6.2(1.5)	6.3(1.4)	.84(.06)	.76(.04)	6.4(.92)	5.4(.66)
GPSM(RSS)-SVI (100,10,3,10,2)	.87(.07)	.91(.07)	5.8(.98)	5.9(.30)	.80(.06)	.85(.05)	5.8(.40)	5.7(.64)
GPSM(RSS)-SVI (100,10,3,10,4)	.87(.06)	.90(.07)	5.9(.94)	5.9(.54)	.82(.06)	.87 (.07)	6.0(1.1)	5.6(.49)

Table 1: We report the result of a scalable Learning experiment for Q1. #T and #L denote the length of full and batch sequence, respectively. #SPPt denotes the number of sampled spectral points of each Gaussian distribution for SM kernel. This means that a total of #SPPt \times Q spectral points are sampled for approximated SM kernel as one hidden state. #B-K and #SPPt-K denote the number of the sampled batch.

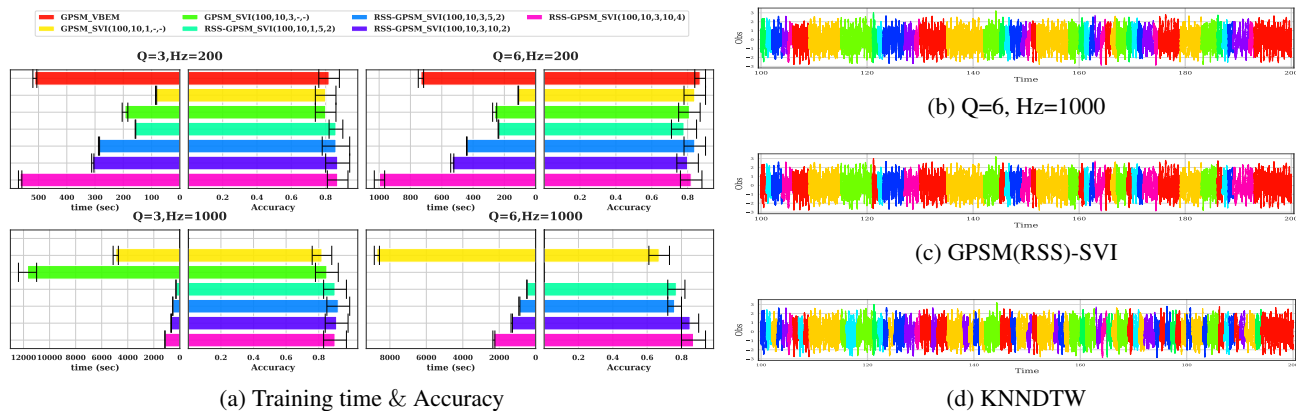


Figure 3: (a) describes the results of the experiments for Hz=200 and Hz=1000 for Q1. This reveals the improvement by SVI and SM approximation through reparameterized RFF, respectively. Figures (b),(c), and (d) show the state Estimation Result for sinusoidal dataset Q=6,Hz=1000. (b),(c), and (d) correspond to the true coloring of testset and GPSM(RSS)-SVI and KNNDTW with accuracy .94 and .69, respectively.

- HMM-T : Vanilla HMM with Multivariate Gaussian emission for time-series observation
- HMM-S : Vanilla HMM with Multivariate Gaussian emission model for spectral density observation by Discrete Fourier Transform
- BHMM-T : Bayesian HMM with Multivariate Gaussian emission for time-series observation
- BHMM-S : Bayesian HMM with Multivariate Gaussian emission model for spectral density observation by Discrete Fourier Transform

We also consider a K-Nearest-Neighbors using Dynamic Time Warping (KNNDTW) which is commonly used for time-series clustering.

- KNNDTW : K-Nearest-Neighbors based on Dynamic

Time Warping [31, 32]

Table 1 reports the statistics of the mean and standard deviation for the accuracy and the number of estimated hidden states computed by 10 repetitive experiments. In terms of accuracy for the state estimation, the HMM-based on GPSM has comparable results with a vanilla version of HMM when $Q = 3$ (data pattern is simple); however, the HMM-based on GPSM has the highest accuracy when $Q = 6$ (data pattern is complex). Figure 3, (a) shows clearly how the proposed training strategy (SVI+R-RFF) reduces the computational time without sacrificing accuracy. The reduction is especially significant when the number of data points in the time series is large. Figures 3, (b), (c), and (d) shows the results of clustering for a different

model, showing that the proposed method matches the true labels quite well.

4.2 Robust State Estimation (Q2)

In HMM research, handling the incomplete dataset containing missing values has been recognized as an important research topic because missing values induces the difficulty of training HMM and estimating the hidden state. To tackle this problem, YEH et al. have investigated how missing data affect the estimation of the HMM parameters in a clinical dataset where missing values are commonly found in the dataset [33]. Popov et al. propose the algorithms of training HMM on sequence data set with missing values by marginalizing the likelihood of missing values for emission [34]. Uvarov et al. develop the modified Viterbi algorithms of HMM for the imputation of incomplete motion data [11].

In this experiment, we aim to evaluate how the HMM-GPSM trained by our proposed learning methods is robust with missing values in the large scale time-series dataset.

We use the PigArtPressure dataset from The UCR time series archive [35]. This data set contains 312 Arterial-blood-pressure time-series data measured at different conditions. This dataset consists of 52 classes, and one time-series of each class has 2000 data points. For the experiment, we randomly chose the 10 class as the hidden state, and sample the observations from the bags of each class. To introduce state transition, we assign Markov assumption over each class. The probability of move and stay over each class is 0.5, respectively. This setting intends to reflect the interesting topic of recognizing the difference between stay and move for dynamic object [36, 37]. Then, we down-sample the timestamps into a half and then use the training set (100×1000) and test set (50×1000).

For comparison, we take GPSM(RSS)-SVI for our approach. Also, KNNDTW, HMM-S, BHMM-T, and BHMM-S which are used in previous experiment 4.1, are compared again. Additionally, we consider the IOHMM [38, 39] that has a different structure of HMM to specifically consider the relation between the inputs and outputs in emission:

- IOHMM : Input and Output HMM with Autoregressive Gaussian emission which assigns the inputs and outputs as spectral density observations and time-series observations

To make missing values in the dataset, we consider two different scenarios; 1) Randomly Missing (RM) that missing values are on randomly chosen timestamps, 2) Interval Missing (IM) that missing values consists of the intervals. We consider the two types of missing percentage $\{25, 50\}$ over each 1000 time-series observations.

To process missing values for other benchmark models, we

Option	PigArtPressure Set					OUR
	KNNDTW	HMM-S	B-HMM-T	B-HMM-S	IOHMM	
N	.58	.57(.05)	.40	.58	.44	.62(.05)
RM25-FO	.61(.02)	.56(.01)	.40	.58	.40(.03)	.61(.06)
RM25-NFO	—	—	—	—	—	.58(.04)
RM50-FO	.60(.02)	.57(.03)	.40(.01)	.58(.04)	.42(.04)	.59(.04)
RM50-NFO	—	—	—	—	—	.61(.05)
IM25-FO	.43(.03)	.46(.07)	.37(.04)	.52(.05)	.35(.04)	.62(.07)
IM25-NFO	—	—	—	—	—	.59(.05)
IM50-FO	.36(.01)	.40(.05)	.31(.03)	.41(.03)	.34(.03)	.57(.03)
IM50-NFO	—	—	—	—	—	.59(.07)

Table 2: Estimation Result for PigArtPressure dataset including missing values (Q2)

consider the conventional Fill-Out (FO) technique [34] that recovers the missing value as the value of the nearest observation. In the case of our model, we also test the incomplete dataset without FO, which corresponds to NFO.

Table 2 compares the mean accuracy and the standard error for hidden state clustering, which are computed from 10 repetitive test experiments. For the RM case, all models achieve the clustering performance as good as the performance on the fully-observed dataset, implying that the FO technique is effective in filling missing observations for the RM case. However, for the IM case, the FO technique does not achieve good performance for simple HMM models and KNNDTW anymore; only our model can maintain the clustering accuracy both for IM25 and IM50. Note that Our method can even maintain the clustering performance even without applying FO techniques, which is impossible for simple HMM models and KNNDTW.

5 Conclusion

We propose the scalable learning method for HMM-GPSM by combining SVI for a long sequence of state transition and R-RFF for a large number of time-series for GP emission. In experiments, we validate that the proposed learning method reduces learning time and estimates the state even though the dataset includes missing values.

In future research, we consider two research directions. First, we will extend the kernel’s expressive power from stationary to non-stationary to overcome the limitation in modeling real data with a stationary kernel [40, 41, 42]. Second, we will relax the Markovian assumption over the transition of the hidden state by considering the complex sequence model such as RNN to figure out the complicated sequential relationship [43, 44, 45].

References

- [1] Mark Gales, Steve Young, et al. The application of hidden markov models in speech recognition. *Foundations and Trends® in Signal Processing*, 1(3):195–304, 2008.
- [2] Junji Yamato, Jun Ohya, and Kenichiro Ishii. Recognizing human action in time-sequential images using hidden markov model. In *Proceedings 1992 IEEE Computer Society conference on computer vision and pattern recognition*, pages 379–385. IEEE, 1992.
- [3] Mohiuddin Ahmad and Seong-Whan Lee. Hmm-based human action recognition using multiview image sequences. In *18th International Conference on Pattern Recognition (ICPR'06)*, volume 1, pages 263–266. IEEE, 2006.
- [4] Jie Yang, Yangsheng Xu, and Chiou S Chen. Human action learning via hidden markov model. *IEEE Transactions on Systems, Man, and Cybernetics-Part A: Systems and Humans*, 27(1):34–44, 1997.
- [5] David Kulp David Haussler and Martin G Reese Frank H Eeckman. A generalized hidden markov model for the recognition of human genes in dna. In *Proc. int. conf. on intelligent systems for molecular biology, st. louis*, pages 134–142, 1996.
- [6] Longfei Li, Yong Zhao, Dongmei Jiang, Yanning Zhang, Fengna Wang, Isabel Gonzalez, Enescu Valentin, and Hichem Sahli. Hybrid deep neural network–hidden markov model (dnn-hmm) based speech emotion recognition. In *2013 Humaine Association Conference on Affective Computing and Intelligent Interaction*, pages 312–317. IEEE, 2013.
- [7] Duc Le and Emily Mower Provost. Emotion recognition from spontaneous speech using hidden markov models with deep belief networks. In *2013 IEEE Workshop on Automatic Speech Recognition and Understanding*, pages 216–221. IEEE, 2013.
- [8] Min Yang. Deep markov neural network for sequential data classification. In *Proceedings of the 53rd Annual Meeting of the Association for Computational Linguistics and the 7th International Joint Conference on Natural Language Processing (Volume 2: Short Papers)*, pages 32–37, 2015.
- [9] Rahul G Krishnan, Uri Shalit, and David Sontag. Structured inference networks for nonlinear state space models. In *AAAI*, 2017.
- [10] Ke Tran, Yonatan Bisk, Ashish Vaswani, Daniel Marcu, and Kevin Knight. Unsupervised neural hidden markov models. *arXiv preprint arXiv:1609.09007*, 2016.
- [11] VE Uvarov, AA Popov, and TA Gulyaeva. Imputation of incomplete motion data using hidden markov models. In *Journal of Physics: Conference Series*, volume 1210, page 012151. IOP Publishing, 2019.
- [12] Tomoaki Nakamura, Takayuki Nagai, Daichi Mochihashi, Ichiro Kobayashi, Hideki Asoh, and Masahide Kaneko. Segmenting continuous motions with hidden semi-markov models and gaussian processes. *Frontiers in neurorobotics*, 11:67, 2017.
- [13] Zitao Liu, Lei Wu, and Milos Hauskrecht. State space gaussian process prediction. In *Proceedings of ICML Workshop on Clinical Data Analysis*. Citeseer, 2012.
- [14] James Hensman, Neil D Lawrence, and Magnus Rattray. Hierarchical bayesian modelling of gene expression time series across irregularly sampled replicates and clusters. *BMC bioinformatics*, 14(1):252, 2013.
- [15] Andrew Wilson and Ryan Adams. Gaussian process kernels for pattern discovery and extrapolation. In *International Conference on Machine Learning*, pages 1067–1075, 2013.
- [16] Kyle R Ulrich, David E Carlson, Wenzhao Lian, Jana S Borg, Kafui Dzirasa, and Lawrence Carin. Analysis of brain states from multi-region lfp time-series. In *Advances in Neural Information Processing Systems*, pages 2483–2491, 2014.
- [17] Kyle R Ulrich, David E Carlson, Kafui Dzirasa, and Lawrence Carin. Gp kernels for cross-spectrum analysis. In *Advances in neural information processing systems*, pages 1999–2007, 2015.
- [18] Matthew D Hoffman, David M Blei, Chong Wang, and John Paisley. Stochastic variational inference. *The Journal of Machine Learning Research*, 14(1):1303–1347, 2013.
- [19] Matthew Johnson and Alan Willsky. Stochastic variational inference for bayesian time series models. In *International Conference on Machine Learning*, pages 1854–1862, 2014.
- [20] Nick Foti, Jason Xu, Dillon Laird, and Emily Fox. Stochastic variational inference for hidden markov models. In *Advances in neural information processing systems*, pages 3599–3607, 2014.
- [21] Matthew James Beal et al. *Variational algorithms for approximate Bayesian inference*. university of London London, 2003.
- [22] Lexing Xie, Shih-Fu Chang, Ajay Divakaran, and Huifang Sun. Learning hierarchical hidden markov models for video structure discovery. *ADVENT Group, Columbia Univ., New York, Tech. Rep*, 6, 2002.

- [23] Carl Edward Rasmussen. Gaussian processes in machine learning. In *Summer School on Machine Learning*, pages 63–71. Springer, 2003.
- [24] Salomon Bochner. *Lectures on Fourier integrals*. Princeton University Press, 1959.
- [25] Ali Rahimi and Benjamin Recht. Random features for large-scale kernel machines. In *Advances in neural information processing systems*, pages 1177–1184, 2008.
- [26] Russel E Caflisch. Monte carlo and quasi-monte carlo methods. *Acta numerica*, 7:1–49, 1998.
- [27] Joaquin Quiñonero-Candela, Carl Edward Rasmussen, Anbal R Figueiras-Vidal, et al. Sparse spectrum gaussian process regression. *Journal of Machine Learning Research*, 11(Jun):1865–1881, 2010.
- [28] David S Watkins. *Fundamentals of matrix computations*, volume 64. John Wiley & Sons, 2004.
- [29] Diederik P Kingma and Max Welling. Auto-encoding variational bayes. *arXiv preprint arXiv:1312.6114*, 2013.
- [30] James Munkres. Algorithms for the assignment and transportation problems. *Journal of the society for industrial and applied mathematics*, 5(1):32–38, 1957.
- [31] Yasushi Sakurai, Christos Faloutsos, and Masashi Yamamuro. Stream monitoring under the time warping distance. In *2007 IEEE 23rd International Conference on Data Engineering*, pages 1046–1055. IEEE, 2007.
- [32] Hui-Huang Hsu, Andy C Yang, and Ming-Da Lu. Knn-dtw based missing value imputation for microarray time series data. *Journal of computers*, 6(3):418–425, 2011.
- [33] Hung-Wen Yeh, Wenyaw Chan, and Elaine Symaniski. Intermittent missing observations in discrete-time hidden markov models. *Communications in Statistics-Simulation and Computation*, 41(2):167–181, 2012.
- [34] Alexander A Popov, Tatyana A Gulyaeva, and Vadim E Uvarov. Training hidden markov models on incomplete sequences. In *2016 13th International Scientific-Technical Conference on Actual Problems of Electronics Instrument Engineering (APEIE)*, volume 2, pages 317–320. IEEE, 2016.
- [35] Hoang Anh Dau, Anthony Bagnall, Kaveh Kamgar, Chin-Chia Michael Yeh, Yan Zhu, Shaghayegh Gharghabi, Chotirat Ann Ratanamahatana, and Eamonn Keogh. The ucr time series archive. *arXiv preprint arXiv:1810.07758*, 2018.
- [36] Davide Anguita, Alessandro Ghio, Luca Oneto, Xavier Parra, and Jorge L Reyes-Ortiz. Human activity recognition on smartphones using a multiclass hardware-friendly support vector machine. In *International workshop on ambient assisted living*, pages 216–223. Springer, 2012.
- [37] David Hallac, Sagar Vare, Stephen Boyd, and Jure Leskovec. Toeplitz inverse covariance-based clustering of multivariate time series data. In *Proceedings of the 23rd ACM SIGKDD International Conference on Knowledge Discovery and Data Mining*, pages 215–223. ACM, 2017.
- [38] Yoshua Bengio and Paolo Frasconi. An input output hmm architecture. In *Advances in neural information processing systems*, pages 427–434, 1995.
- [39] Silvia Chiappa and Samy Bengio. Hmm and iohmm modeling of eeg rhythms for asynchronous bci systems. Technical report, IDIAP, 2003.
- [40] Sami Remes, Markus Heinonen, and Samuel Kaski. Non-stationary spectral kernels. In *Advances in Neural Information Processing Systems*, pages 4642–4651, 2017.
- [41] Sami Remes, Markus Heinonen, and Samuel Kaski. Neural non-stationary spectral kernel. *arXiv preprint arXiv:1811.10978*, 2018.
- [42] Jean-Francois Ton, Seth Flaxman, Dino Sejdic, and Samir Bhatt. Spatial mapping with gaussian processes and nonstationary fourier features. *Spatial statistics*, 28:59–78, 2018.
- [43] Hanjun Dai, Bo Dai, Yan-Ming Zhang, Shuang Li, and Le Song. Recurrent hidden semi-markov model. 2016.
- [44] Scott W Linderman, Andrew C Miller, Ryan P Adams, David M Blei, Liam Paninski, and Matthew J Johnson. Recurrent switching linear dynamical systems. *arXiv preprint arXiv:1610.08466*, 2016.
- [45] Scott Linderman, Matthew Johnson, Andrew Miller, Ryan Adams, David Blei, and Liam Paninski. Bayesian learning and inference in recurrent switching linear dynamical systems. In *Artificial Intelligence and Statistics*, pages 914–922, 2017.

6 Supplementary Material

6.1 Derivation

6.1.1 SVI application to Bayesian HMM with GP emission

We derive (1) how the ELBO of the full sequence of time series data is linearly approximated by the ELBO of the batch sequence of time series data and (2) how the batch factors introduced in Section 3.1 are derived.

Given the sampled $i \in \{1, \dots, T - L + 1\}$ uniformly, let $Y_L^s = \{y_{i,:}, \dots, y_{i+L-1,:}\}$ be sampled observation with the length L and X_L^s be corresponding inputs and Z_L^s corresponding hidden states. The expected log joint likelihood of $\{Z_L^s, Y_L^s\}$ given X_L^s is approximated as

$$\begin{aligned}
 & \mathbb{E}_s \left[\mathbb{E}_q [\log p(Y_L^s, Z_L^s | X_L^s)] \right] \\
 &= \sum_{i=0}^{T-L} \frac{1}{T-L+1} \mathbb{E}_q [\log p(Y_L^{s_i}, Z_L^{s_i} | X_L^{s_i})] \\
 &= \frac{1}{T-L+1} \sum_{i=0}^{T-L} \mathbb{E}_q \left[\log p(z_i) + \underbrace{\sum_{t=1}^L \log p(A_{z_{i+t-1}, z_{i+t}})}_{\text{transition term}} + \underbrace{\sum_{t=1}^L \log p(y_{i+t,:} | z_{i+t}, x_{i+t,:})}_{\text{observation term}} \right] \cdots (*) \\
 &\approx \frac{1}{T-L+1} \mathbb{E}_q \left[\sum_{t=1}^{T-L+1} \log p(z_{t-1}) + L \sum_{t=1}^T \log p(A_{z_{t-1}, z_t}) + L \sum_{t=1}^T \log p(y_{t,:} | z_t, x_{t,:}) \right]
 \end{aligned}$$

This implies that transition and observation term of $\mathbb{E}_q[\log p(Y_L^s, Z_L^s | X_L^s)]$ for the sampled $i \in \{1, \dots, T - L + 1\}$ can be approximated as

$$\begin{aligned}
 \mathbb{E}_q \left[\sum_{t=1}^L \log p(A_{z_{i+t-1}, z_{i+t}}) \right] &\approx \frac{L}{T-L+1} \mathbb{E}_q \left[\sum_{t=1}^T \log p(A_{z_{t-1}, z_t}) \right] \\
 \mathbb{E}_q \left[\sum_{t=1}^L \log p(y_{i+t,:} | z_{i+t}, x_{i+t,:}) \right] &\approx \frac{L}{T-L+1} \mathbb{E}_q \left[\sum_{t=1}^T \log p(y_{t,:} | z_t, x_{t,:}) \right]
 \end{aligned}$$

Thus, the batch factors, c_s^A and c_s^θ , to calibrate the approximated ELBO are obtained as

$$c_s^A = \frac{T-L+1}{L}, \quad c_s^\theta = \frac{T-L+1}{L}$$

The transition term in expectation in (*) can be approximated as

$$\begin{aligned}
 \sum_{i=0}^{T-L} \mathbb{E}_q \left[\sum_{t=1}^L \log p(A_{z_{i+t-1}, z_{i+t}}) \right] &= \mathbb{E}_q \left[\sum_{j=1}^L \log p(A_{z_{j-1}, z_j}) + \sum_{j=2}^{L+1} \log p(A_{z_{j-1}, z_j}) + \cdots + \sum_{j=T-L+1}^T \log p(A_{z_{j-1}, z_j}) \right] \\
 &= \mathbb{E}_q \left[L \sum_{t=L}^{T-L+1} \log p(A_{z_{t-1}, z_t}) + \underbrace{\sum_{t=1}^{L-1} t (\log p(A_{z_{t-1}, z_t}) + \log p(A_{z_{T-t}, z_{T-t+1}}))}_{\text{approximated term}} \right] \\
 &\approx \mathbb{E}_q \left[L \sum_{t=L}^{T-L+1} \log p(A_{z_{t-1}, z_t}) + L \sum_{t=1}^{L-1} (\log p(A_{z_{t-1}, z_t}) + \log p(A_{z_{T-t}, z_{T-t+1}})) \right] \\
 &= \mathbb{E}_q \left[L \sum_{t=1}^T \log p(A_{z_{t-1}, z_t}) \right]
 \end{aligned}$$

Here, the observation term in expectation in (*) can be approximated as

$$\begin{aligned}
 & \sum_{i=0}^{T-L} \mathbb{E}_q \left[\sum_{t=1}^L \log p(y_{i+t,:} | z_{i+t}, x_{i+t,:}) \right] = \mathbb{E}_q \left[\sum_{j=1}^L \log p(y_{j,:} | z_j, x_{j,:}) + \cdots + \sum_{j=T-L+1}^T \log p(y_{j,:} | z_j, x_{j,:}) \right] \\
 & = \mathbb{E}_q \left[L \sum_{t=L}^{T-L+1} \log p(y_{t,:} | z_t, x_{t,:}) + \underbrace{\sum_{t=1}^{L-1} t (\log p(y_{t,:} | z_t, x_{t,:}) + \log p(y_{T-t+1,:} | z_{T-t+1}, x_{T-t+1,:}))}_{\text{approximated term}} \right] \\
 & \approx \mathbb{E}_q \left[L \sum_{t=L}^{T-L+1} \log p(y_{t,:} | z_t, x_{t,:}) + L \sum_{t=1}^{L-1} (\log p(y_{t,:} | z_t, x_{t,:}) + \log p(y_{T-t+1,:} | z_{T-t+1}, x_{T-t+1,:})) \right] \\
 & = \mathbb{E}_q \left[L \sum_{t=1}^T \log p(y_{t,:} | z_t, x_{t,:}) \right]
 \end{aligned}$$

6.1.2 Reparameterized RFF SM kernel approximation

Given the parameters of SM kernel $\{w_q, \mu_q, \sigma_q\}_{q=1}^Q$, we sample spectral points from Gaussian distribution $p^{(q)}(S) = N(S; \mu_q, \sigma_q)$ by reparametrization trick.

$$s_{q,i} = \mu_q + \sigma_q \circ \epsilon_i$$

where $\epsilon_i \sim N(\epsilon; 0, I)$ for $i = 1, \dots, m_q$.

If we define the $x_{S^{(q)}} = [2\pi x^T s_{q,1}, \dots, 2\pi x^T s_{q,m_q}]$ and the feature map $\phi_q(x) = \frac{1}{\sqrt{m_q}} [\cos(x_{S^{(q)}}), \sin(x_{S^{(q)}})]$, then $\phi_q(x)\phi_q(y)^T$ can approximate $k_q(x-y)$ that is the induced kernel from Gaussian Spectral density $p^{(q)}(S)$ by Bochner's theorem.

$$\begin{aligned}
 \mathbb{E}_{p^{(q)}(S)} [\phi_q(x)\phi_q(y)^T] &= \mathbb{E}_{p^{(q)}(S)} \left[\frac{1}{m_q} \sum_{i=1}^{m_q} (\cos 2\pi s_{(q,i)}^T x) (\cos 2\pi s_{(q,i)}^T y) + (\sin 2\pi s_{(q,i)}^T x) (\sin 2\pi s_{(q,i)}^T y) \right] \\
 &= \mathbb{E}_{p^{(q)}(S)} \left[\frac{1}{m_q} \sum_{i=1}^{m_q} \cos 2\pi s_{(q,i)}^T (x-y) \right] \\
 &= \mathbb{E}_{p^{(q)}(S)} \left[\frac{1}{m_q} \sum_{i=1}^{m_q} \frac{e^{i2\pi s_{(q,i)}^T (x-y)} + e^{-i2\pi s_{(q,i)}^T (x-y)}}{2} \right] \\
 &= \frac{1}{2} (k_q(x-y) + k_q(y-x)) = \frac{1}{2} (k_q(x-y) + k_q(x-y)) \\
 &= k_q(x-y)
 \end{aligned}$$

Using the above derivation, we define sampled spectral points $\mathbf{s} = \cup_{q=1}^Q \{s_{q,i}\}_{i=1}^{m_q}$ from $p(S) = \prod_{q=1}^Q p^{(q)}(S)$ and the feature map $\phi_{SM}(x) = [\sqrt{w_1}\phi_1(x), \dots, \sqrt{w_Q}\phi_Q(x)]$, which can approximate $k_{SM}(x, y)$ by $\phi_{SM}(x)\phi_{SM}(y)^T$.

$$\begin{aligned}
 \mathbb{E}_{p(S)} [\phi_{SM}(x)\phi_{SM}(y)^T] &= \mathbb{E}_{p(S)} \left[\sum_{q=1}^Q w_q \phi_q(x)\phi_q(y)^T \right] \\
 &= \sum_{q=1}^Q w_q \mathbb{E}_{p^{(q)}(S)} [\phi_q(x)\phi_q(y)^T] \\
 &= \sum_{q=1}^Q w_q k_q(x-y) = k_{SM}(x-y)
 \end{aligned}$$

6.1.3 Regularized Lower bound for GP emission

We consider the lower bound of log marginal likelihood with the candidate distribution $q(S)$. We can derive the lower bound \mathcal{L} as follows:

$$\begin{aligned}
 \log p(Y|X) &= \log \iint p(Y|f)p(f|X, S) \frac{p(S)}{q(S)} q(S) df dS \\
 &= \log \int p(Y|X, S) \frac{p(S)}{q(S)} q(S) dS \\
 &\geq \int \log \left(p(Y|X, S) \frac{p(S)}{q(S)} \right) q(S) dS \\
 &= \int \log p(Y|X, S) q(S) + \log \frac{p(S)}{q(S)} q(S) dS \\
 &= \int \log p(Y|X, S) q(S) dS - KL(q(S)||P(S)) = \mathcal{L}
 \end{aligned}$$

Applying the Stochastic Gradient Variational Bayes (SGVB) [29] to \mathcal{L} with the reparametrizable distribution $q(S)$, leads to the following unbiased estimator $\hat{\mathcal{L}}_K$.

$$\hat{\mathcal{L}}_K = \frac{1}{K} \sum_{i=1}^K \log p(Y|X, s^{(i)}) - KL(q(S)||P(S))$$

where $s^{(i)}$ is i -th sampled spectral points from $q(S)$.

6.2 Algorithm

6.2.1 Initialization of SM Kernel hyperparameters

Algorithm 1: SM Kernel parameters initialization for Clustering

Input : Data : $X = \{x_{t,:}\}_{t=1}^T$ and $Y = \{y_{t,:}\}_{t=1}^T$
 K : #Cluster , Q : #Mixture Component for SM kernel
Output: $\theta = \{\{w_q^k, \mu_q^k, \sigma_q^k\}\}_{q=1, k=1}^{Q, K}$
for $t=1, \dots, T$ **do**
| Get the normalized empirical spectral density s_t from y_t by FFT
end
Get the mean of $\{m_k\}_{k=1}^K$ for each cluster after applying k-means clustering s_t
for $k=1, \dots, K$ **do**
| Get the cumulative distribution function (CDF) of m_k by applying CumSum to m_k
| Sample the spectral points by applying inverse sampling the CDF of m_k
| Fit the Gaussian Mixture distribution (GMM) by the sampled spectral points
| Obtain k th SM kernel parameters $\{w_q^k, \mu_q^k, \sigma_q^k\}_{q=1}^Q$
end
Get the initial SM hyperparameters $\{w_q^k, \mu_q^k, \sigma_q^k\}_{q=1, k=1}^{Q, K}$

6.2.2 GPSM(RSS)-SVI

Algorithm 2: GPSM(RSS)-SVI Learning

Input : Data : $X = \{x_{t,:}\}_{t=1}^T$ and $Y = \{y_{t,:}\}_{t=1}^T$,
 K : #Cluster , Q : #Mixture Component for SM kernel,
 L : the length of sampled sequence , M : #batch for sampled sequence
 m : #Spectral point for SM kernel approximation
Output: $\theta^* = \{\{w_q^k, \mu_q^k, \sigma_q^k\}\}_{q=1, k=1}^{Q, K}$, w_π^* , and w_A^*
Initialize SM kernel hyperparameter θ by **Algorithm 1**
while *not converged* **do**
| Sample the m batch data $\{Y_L^{s_m}, X_L^{s_m}\}_{m=1}^M$
| # Local Variable Parameter Update
| **for** $m = 1 : M$ **do**
| | Calculate $q^*(Z_L^{s_m})$ for $\{Y_L^{s_m}, X_L^{s_m}\}$ by with equation (17) and (18)
| **end**
| # Global Variable Parameter Update
| Update w_{p_i} and w_A by equation (27) and (28)
| Update SM kernel hyperparameters θ by applying ADAM to the equation (29)
| except that $\log(p(y_{i+t,:}, z_{i+t}, y_{i+t,:}))$ in (29) is replaced by the equation (32)
end

6.3 Experiments

6.3.1 Scalable Learning (Q1)

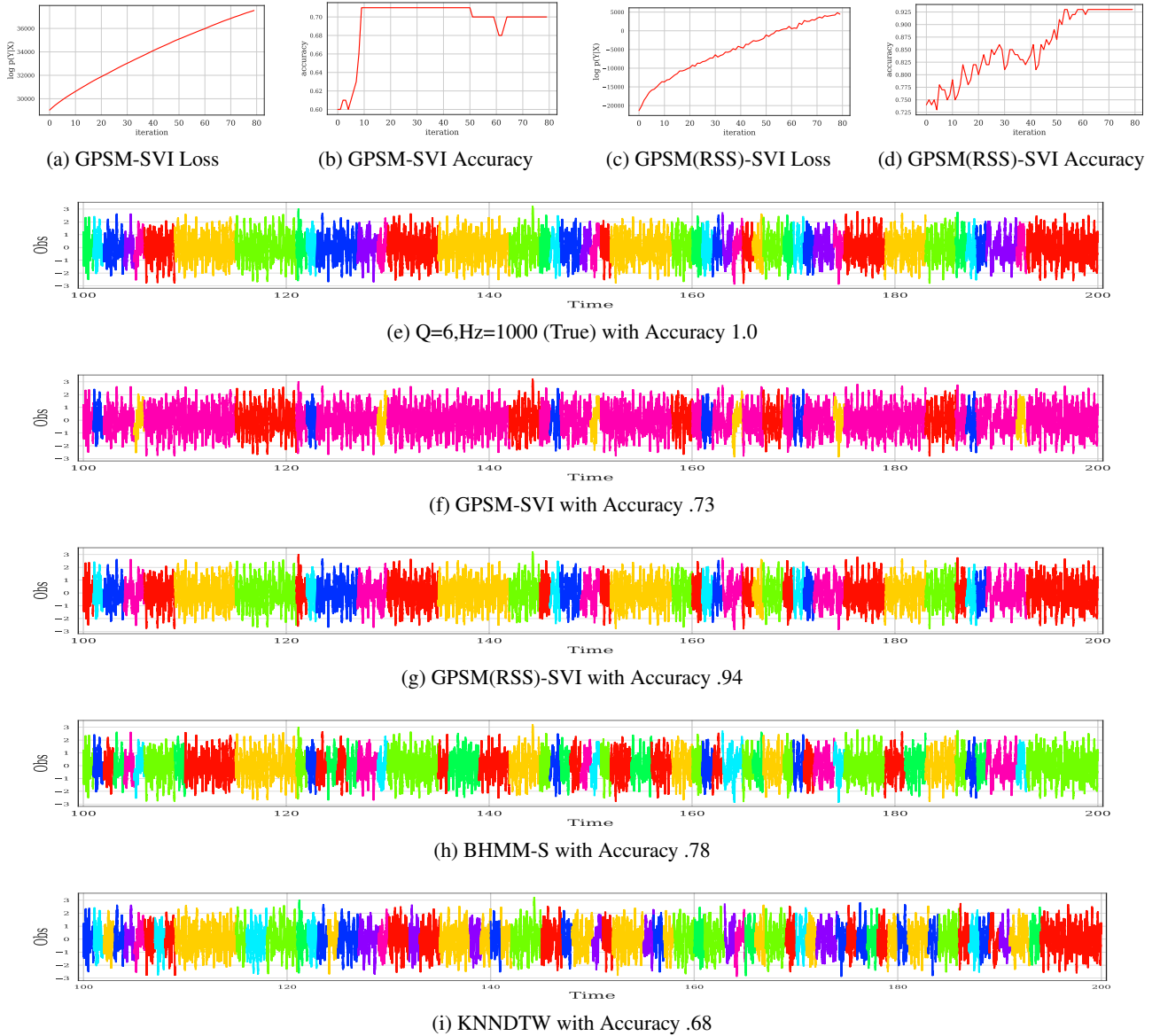


Figure 4: We describe the scalable learning experiment result for the case of $Q = 6, Hz = 1000$. Our models are trained during 80 iterations until the models arrive at local optimal. Figures (a) and (c) show the log marginal likelihood $\log p(Y|X)$ of GPSM-SVI and GPSM(RSS)-SVI during training. Figures (b) and (d) show the change of the training Accuracy during training. Figures (e), (f), (g), (h), and (i) shows each model’s clustering result for test data along with Accuracy.

6.3.2 Robust State Estimation (Q2)

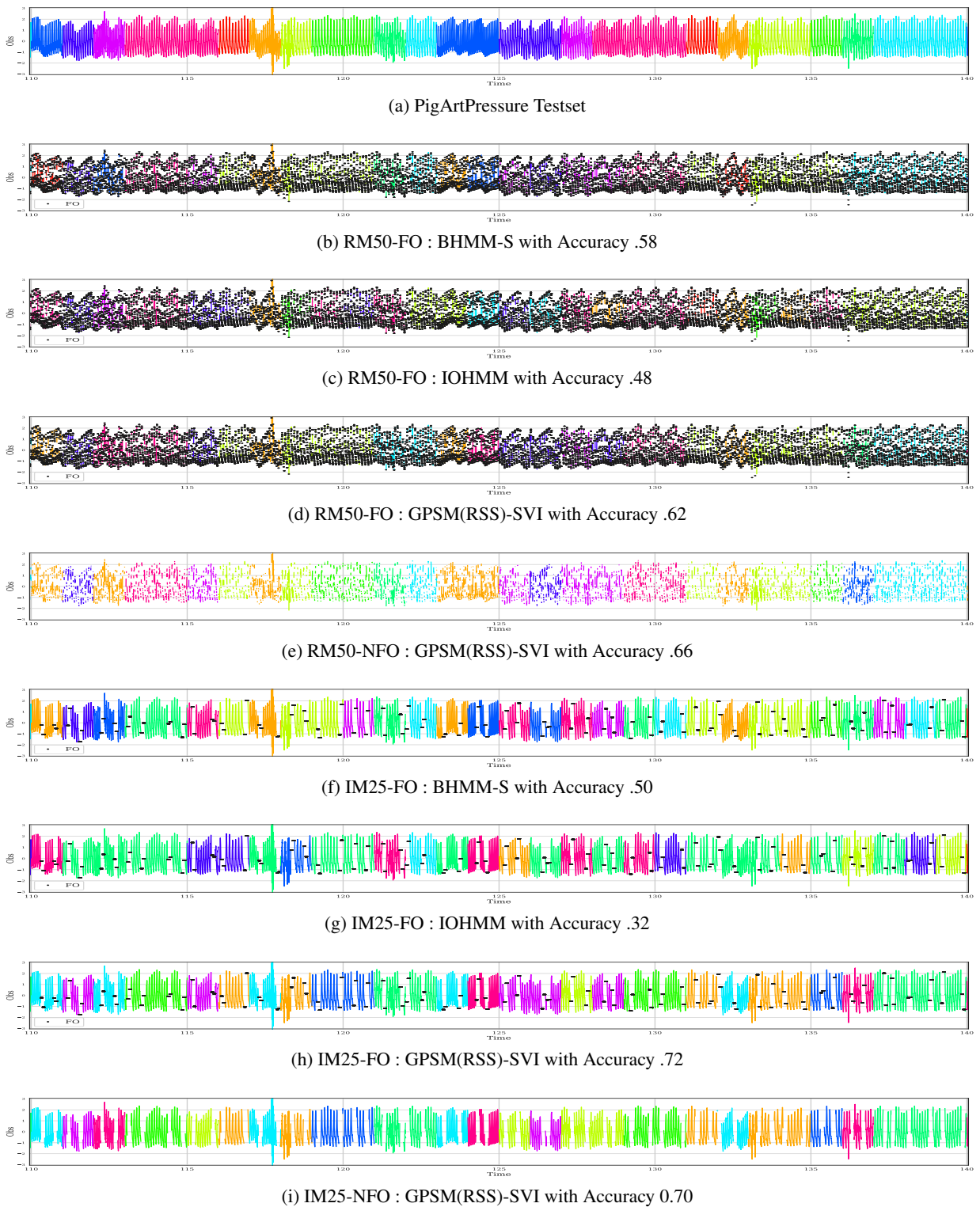


Figure 5: We describe the state estimation result for experiment 2 (Robust estate estimation). Figure (a) shows a subset of test data within the time interval $[110,140]$ out of test data set $[100,150]$. Figures (b),(c), and (d) show the results of the clustering task for the case of RM50 with the FO technique. Figure (e) shows the clustering results for GPSM(RSS)-SVI (our proposed method) without using FO. Similarly, Figures (f),(g), and (h) show the results for IM25. Figure (i) shows the clustering result for GPSM(RSS)-SVI (our proposed method) without using the FO technique for IM25.